Kobe University Repository : Kernel

PDF issue: 2025-12-05

Water uptake of porous building materials with extremely small air entrapment effects

Fukui, Kazuma
Takada, Satoru

(Citation)
Journal of Physics: Conference Series,2654:012033

(Issue Date)
2023

(Resource Type)
conference paper

(Version)
Version of Record

(Rights)
© 2023 The Author(s). Published by National Institute for Materials Science in partnership with Taylor & Francis Group.
Content from this work may be used under the terms of the Creative Commons Attribution 3.0 licence. Any further distribution of this work must maintain attribution to the…

(URL)
https://hdl.handle.net/20.500.14094/0100488589

Journal of Physics: Conference Series

PAPER • **OPEN ACCESS**

Water uptake of porous building materials with extremely small air entrapment effects

To cite this article: Kazuma Fukui and Satoru Takada 2023 *J. Phys.: Conf. Ser.* **2654** 012033

View the article online for updates and enhancements.

You may also like

- Effects of structures of microemulsions containing a deep eutectic solvent on the entrapment amount and the skin permeation of resveratrol
Mina Sakuragi, Hana Yoshimura and Katsuki Kusakabe
- Entrapment of Hypervolatiles in Interstellar and Cometary H_2O and CO_2 Ice Analogs
Alexia Simon, Mahesh Rajappan and Karin I. Öberg
- Physiology and biochemistry of human subjects during entrapment
A Agapiou, K Mikedi, S Karma et al.

This content was downloaded from IP address 133.30.169.29 on 10/04/2024 at 05:48

Water uptake of porous building materials with extremely small air entrapment effects

Kazuma Fukui* and Satoru Takada

Graduate School of Engineering, Kobe University, 1-1, Rokkodai-cho, Nada-ku, Kobe, 657-8501, Japan

*fukui@peridot.kobe-u.ac.jp

Abstract. When a porous material is near capillary saturation, entrapped air is expected to affect water transfer through the pores. Based on the results of water absorption tests at reduced air pressure, Janssen et al. (Energy Procedia, 2015) demonstrated that air entrapment prevents water absorption above capillary saturation. In this study, to understand the air entrapment effects on water transfer in the high-water-saturation region, we further examined the water transfer characteristics corresponding to extremely small air entrapment effects. First, using three common porous building materials, water uptake experiments were conducted at low air pressure near vacuum (several kilopascals), and the time evolution of the water absorption was measured. The results show that low air pressure accelerates water uptake by brick and aerated concrete specimens, whereas the water uptake by calcium silicate board specimens is not significantly affected. These differences among the materials are discussed from the viewpoint of the pore structure. Furthermore, the results of simultaneous water and air transfer calculations confirm that air entrapment and pressure development in the pores can significantly reduce the rate of water uptake and the water content that a material can reach after capillary absorption.

1. Introduction

To evaluate the hygrothermal performance of building envelopes with water supply, such as rain and ground water, it is important to understand the water transfer characteristics of porous building materials at high water saturation. In particular, the risks of moisture-relevant problems, such as frost damage, highly depend on the water content in the high-water content region [1].

After free water absorption, porous building materials reach capillary saturation rather than complete saturation. This is most probably because the air remaining in the pores prevents water absorption. Janssen et al. [2] conducted water absorption tests at reduced air pressure. Their results indicated that water absorption at the reduced pressure increased significantly compared to water absorption under atmospheric pressure. Therefore, the influence of air on the water transfer in a material cannot be ignored in a high-water-saturation region.

While two-phase flow is a common problem in soil physics (e.g., [3]), air transfer in porous building materials is only considered under extreme conditions. For example, most material surfaces are sealed for moisture proof which also prevents air movement through the surfaces. In the literature, it has been shown that air that cannot escape from material surfaces affects water absorption when a material is sealed, except on the water-absorbing surface or when the material has a low permeable surface finish [4, 5, 6].

Content from this work may be used under the terms of the Creative Commons Attribution 3.0 licence. Any further distribution of this work must maintain attribution to the author(s) and the title of the work, journal citation and DOI.
Published under licence by IOP Publishing Ltd

To understand the air entrapment effects on water transfer in the high-water saturation region under common water uptake conditions, we further examined the water transfer characteristics corresponding to extremely small air entrapment effects in this study. First, water absorption tests were conducted using several types of porous building materials, namely bricks, autoclaved aerated concrete (AAC), and a calcium silicate board (CS), at reduced air pressure in a vacuum desiccator to compare the time evolution of water absorption with significantly small air entrapment effects with that at the atmospheric pressure. Furthermore, simultaneous water and air transfer calculations were conducted to confirm the effects of air entrapment on water uptake.

2. Water absorption tests at extremely low air pressure

2.1. Methods

Figure 1 compares the pore volume distributions of the three types of materials employed: bricks, AAC, and CS. The bottom surfaces of the specimens had a size of 40 or 50 mm × 60 mm. The height was 100 mm for the brick and CS specimens but 50 mm for AAC, considering its slow absorption. The sides of the specimens were sealed with epoxy resin and aluminum foil. Note that the tests were conducted under ordinal conditions, except for the surrounding air pressure; the specimens had no additional sealing on the top surface or finish layers. The specimens were air dried before the tests.

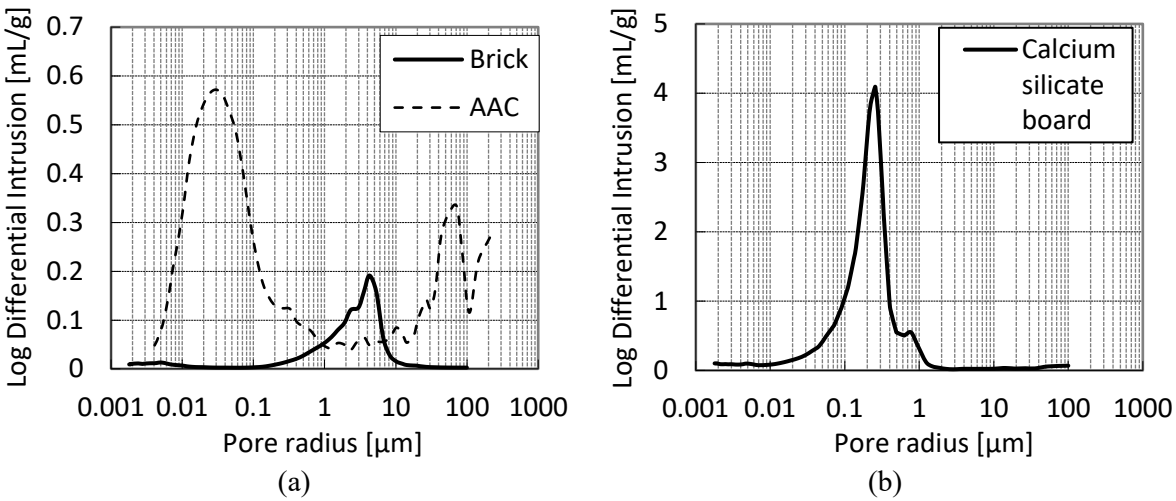

Figure 1. Pore volume distribution of the employed three materials: (a) brick, autoclaved aerated concrete (AAC), and (b) calcium silicate board.

For the brick and CS, two specimens were prepared: one for the test at atmospheric pressure and the other for the tests at reduced air pressure. Before the tests, we confirmed that the absorption rates of the two specimens at atmospheric pressure were similar. Tests using AAC, which has relatively low absorption rates, were conducted using multiple specimens under both atmospheric and low-pressure conditions to confirm the differences among the specimens. Three specimens for the atmospheric pressure and four specimens for the reduced air pressure were prepared.

The tests were conducted in a laboratory at a temperature of 23 °C. The first series of tests was conducted at atmospheric pressure. The second series was conducted in a desiccator in which the air pressure was reduced using a vacuum pump. The pumping speed of the pump was 7 L/min, which maintained the air pressure in the desiccator at several kilopascals. We avoided using a lower pressure to prevent the boiling of water in the reservoir. After reducing the air pressure in the desiccator, water uptake tests were performed by pouring water into the reservoir.

Water was absorbed from the bottom surface of the specimens, while the top surface was exposed to air in the laboratory or desiccator. During the tests at atmospheric pressure, the water uptake was

intermitted several times to weigh the specimens. During the tests at low pressure, the samples were weighed only once for one test to prevent them from being exposed to atmospheric pressure during the water absorption, and the tests were repeated from the air-dry state again to obtain the time evolution of the water absorption.

2.2. Results and discussion

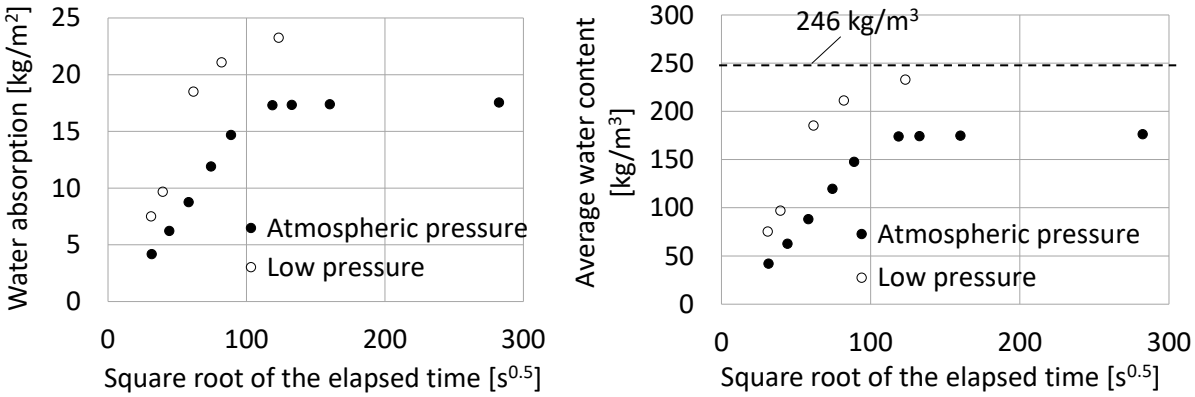

(a)

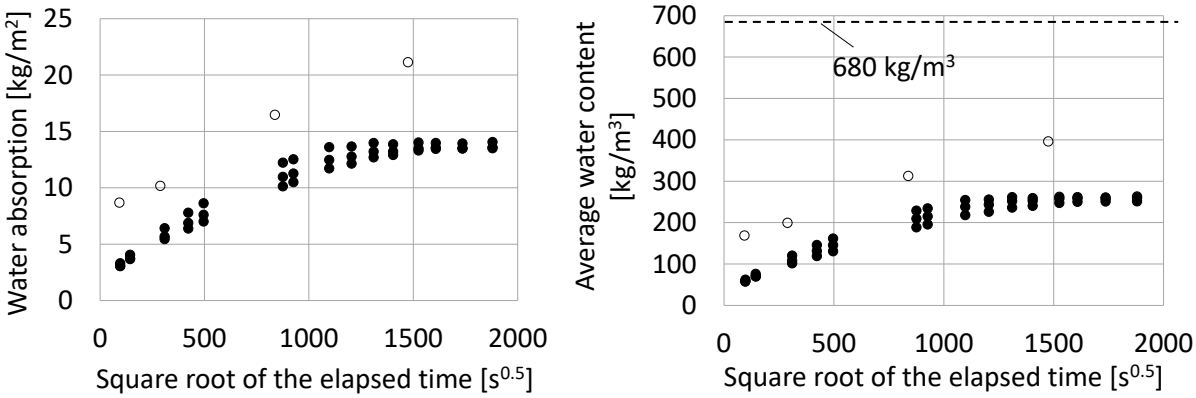

(b)

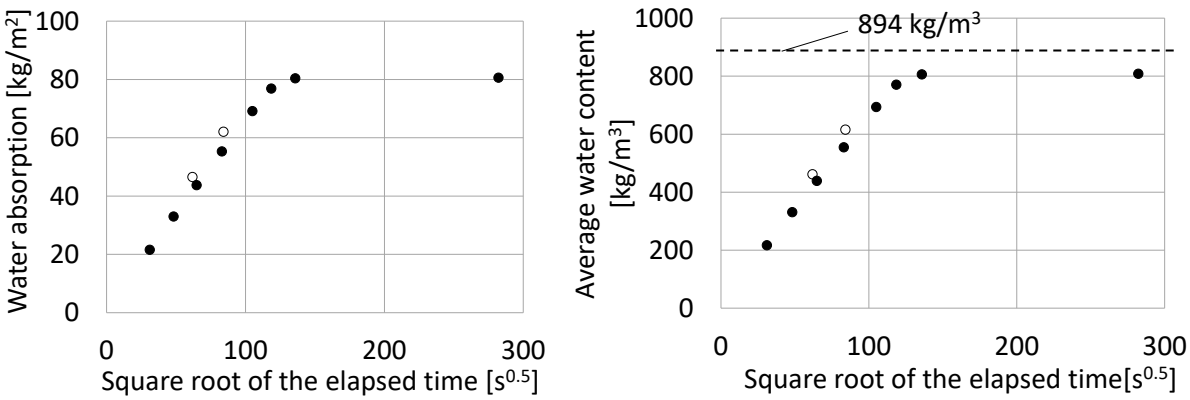

(c)

Figure 2. Time evolution of the mass of the absorbed water and average water content of the (a) brick, (b) autoclaved aerated concrete, and (c) calcium silicate board specimens at atmospheric and extremely low pressure.

Figure 2 compares the time evolution of the absorbed water mass at atmospheric pressure and extremely low air pressure as well as the average water content of the specimens calculated from it. The completely saturated water content of the materials determined from the water content at vacuum saturation or mercury porosimetry is also shown in the right side. While no obvious changes were observed for CS at atmospheric and low pressures, the absorbed water mass at the steady state increased in the case of low air pressure for the brick and AAC specimens, as shown by Janssen et al. [2]. In addition, the results showed that the absorption rates of the brick and AAC specimens increased at low air pressures. The absorption coefficient of the brick became 1.7 times larger at low air pressure. Furthermore, while the water content of the CS was close to the porosity, even at atmospheric pressure, the water content of the brick and AAC was not. The brick specimens reached near-complete saturation only at low air pressure. These results indicated the significance of the effects of air entrapment on water absorption.

To discuss the differences between the materials, we compared the experimental results with those of the pore structure. Based on the Young Laplace equation and Boyle's law, Fagerlund [7] proposed the following equation to predict the extent of air compression in a spherical pore owing to water uptake.

$$\alpha^{1/3}\left(\alpha^{-1}-1\right)=\frac{2\gamma}{p_0 r} \tag{1}$$

Here, p_0 is the air pressure before compression (Pa); r is the pore radius (m); γ is the surface tension (N/m^2); α is the ratio of the compressed air volume V/V_0, where V_0 and V are the air volumes before and after compression, respectively. This equation indicates that the degree of air compression in a pore depends on the pore radius or capillary force. In a finer pore, a large capillary force compresses the entrapped air more significantly.

Using this equation, we determined α both at the atmospheric and low air pressures, as listed in table 1. These values corresponded to the peak radius of the pore volume distribution (figure 1). For AAC, which had the two peaks, the peak at the larger pore radius was selected. CS has smaller pores than other materials. Therefore, the capillary force in the pores is larger, and the sucked water compresses air significantly, even when water uptake occurs at atmospheric pressure. Fagerlund [7] pointed out that the effects of air compression in such small pores on the water uptake should be small because the compressed air volume is small and air dissolution is accelerated owing to the high pressure. Conversely, there are large differences in α at atmospheric and low air pressure for the brick and AAC, which can be a reason for the different water absorption characteristics at different air pressures (figure 2). For the brick, α at a low air pressure is negligibly small, which can be attributed to the high water content near complete saturation after water uptake (figure 2 (a)). AAC has relatively large pores, and even at low pressure, the air is not completely compressed. Therefore, it is considered that some air remained in the pores during the water absorption tests.

Table 1. Peak pore radius and ratio of the compressed air volume α related to the air volume before the compression due to water uptake.

		Brick	Calcium silicate board	AAC
Peak pore radius (μm)		4.27	0.256	71.8
α	Under atmospheric pressure	0.72	0.07	0.98
	Under extremely low pressure (2 kPa)	0.01	0.00	0.40

3. Simultaneous air and water transfer simulation

3.1. Method

3.1.1. Fundamental equations. We performed calculations corresponding to the water uptake of the bricks, as the difference in the water absorption at the atmospheric and extremely low pressure is clear

for the brick according to figure 2 and table 1. The following two equations are the mass conservation equations for air and liquid water in a porous material [6].

$$\frac{\partial \rho_a \psi_a}{\partial t} = \frac{\partial}{\partial z}\left\{\frac{k_a}{g}\left(\frac{\partial p_a}{\partial z} - \rho_a g\right)\right\} \tag{2}$$

$$\frac{\partial \rho_l \psi_l}{\partial t} = \frac{\partial}{\partial z}\left\{\lambda'_P\left(\frac{\partial p_l}{\partial z} - \rho_l g\right)\right\} \tag{3}$$

Here, g is the gravitational acceleration (m/s^2); k_a is the coefficient of air permeability (m/s); p is the pressure (Pa); t is the time (s); z is the position (m); λ'_p is the water conductivity due to the water pressure gradient (kg/(m·s·Pa)), and ψ is the volume fraction (m^3/m^3). The subscripts a and l denote air and liquid water, respectively. The sum of ψ_l and ψ_a is equal to the material porosity, and the air pressure is calculated based on the ideal gas law.

$$p_a \rho_a^{-1} = R_d T \ , \tag{4}$$

where R_d is the gas constant (J/(kg·K)), and T is the temperature (K).

3.1.2. Calculation conditions and cases. The calculations were conducted one dimensionally along the specimen height. Equations (1) and (2) were discretized using the finite difference method. The discretization for the time and space was conducted using the forward and central differences, respectively, and the time and space steps were 1 mm and 5 × 10^{-6} s, respectively. The initial conditions of humidity and air pressure in the material were set to 28% and atmospheric pressure, respectively. On the water absorption surface, the capillary pressure was set to −0.1 kPa, and no air flow was considered. On the surface exposed to air, the air pressure was set to atmospheric pressure. Vapor transfer was considered using the Robin boundary condition with an air humidity of 28%, and the vapor transfer coefficient between the material surface and air was set to 6.77 × 10^{-6} (kg/(m·s(kg/kg))). The temperature of the material and air was set to 23 °C.

We performed the three calculations listed in table 2. The calculation for Cases 1 and 2 was performed to check the validity of the material properties. Material properties are commonly measured at atmospheric pressure and include air entrapment effects implicitly. Therefore, we used two sets of the properties corresponding to atmospheric pressure and extremely low pressure. Calculation Case 1 was based on an ordinal liquid water transfer calculation using material properties mostly measured at the atmospheric pressure. Conversely, calculation Case 3 was based on material properties excluding the air entrapment effects, but it considered air transfer in the material instead, which also corresponded to the water uptake at atmospheric pressure.

Table 2. Calculation conditions.

	Fundamental equations	Air pressure to which material properties correspond	Reproduced water absorption experiments
Case 1	Liquid water transfer	Atmospheric pressure	Experiment at atmospheric pressure
Case 2	Liquid water transfer	Extremely low pressure	Experiment at extremely low pressure
Case 3	Air and liquid water transfer	Extremely low pressure	Experiment at atmospheric pressure

3.1.3. Material properties. The material properties at low pressure near vacuum were derived using a simple assumption in this study. First, the moisture diffusivity was derived using the Ruler method [8]. The method derives the moisture diffusivity without using the Boltzmann transformation of the time

evolution of moisture content distribution during water uptake. In the Ruler method, Boltzmann variable λ_f (m/s$^{0.5}$) at the wetting front is determined from visual observation. An approximate curve for the water content as a function of the Boltzmann variable is then estimated from the water absorption coefficient A (kg/(m^2·s$^{0.5}$)) and two boundary conditions, i.e., $w = 0$ at $\lambda = \lambda_f$ and $w = w_{cap}$ at $\lambda = 0$. A was derived from the results of the water uptake tests, and the maximum water content after water absorption was set to the values at the capillary and complete saturation for the tests at atmospheric and low pressures, respectively. The Boltzmann variation at the wet front was determined using an additional water-uptake test at atmospheric pressure. To apply the value for the low-pressure case, we assumed that the rate of the wetting front movement was inversely proportional to the time until the specimen reached saturation t_{sat} (s), which was determined from the linear approximation of the time evolution of the absorbed water mass as a function of the square root of the elapsed time, as shown in figure 3 (a). The water diffusivity obtained is shown in figure 3 (b). Note that the estimated water diffusivity at low pressure was smaller than that at atmospheric pressure in the region below the capillary saturation, but there is no physical evidence for that. Therefore, the relationship between the water diffusivity under the two conditions should be further examined.

The adsorption isotherm at low air pressure was determined based on [9]; however, the values were multiplied such that the water content at saturation corresponded to that at the complete saturation of the employed material. Considering that the air pressure increased by approximately 39 kPa when compressed until the volume decreased to 72% (table 1), the function for the atmospheric pressure was created such that the water content differed from that of the low air pressure only near saturation (below several kilopascals), as shown in figure 4. Finally, the air permeability is given as a function of the water content, as shown in figure 5, based on the two measured data.

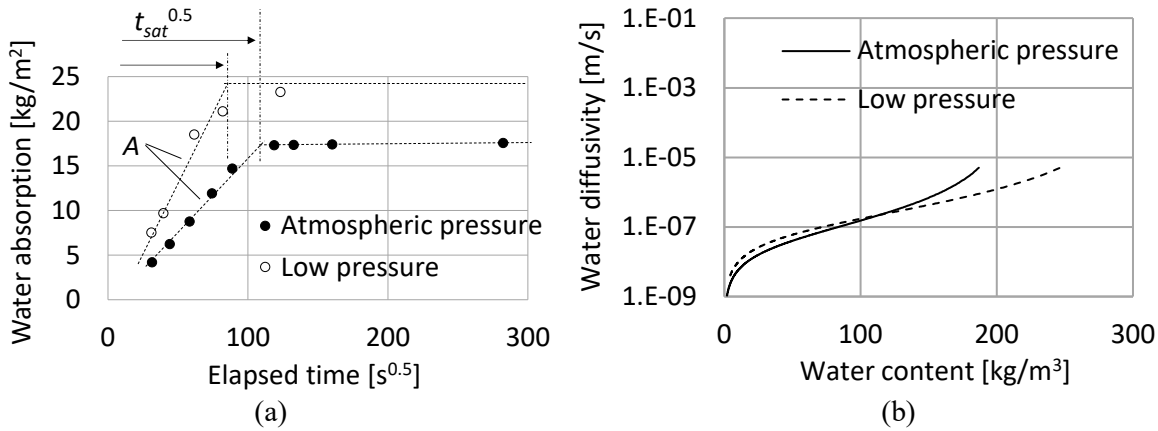

Figure 3. (a) Comparison of the water uptake at the atmospheric and extremely low air pressure and (b) derived water diffusivity.

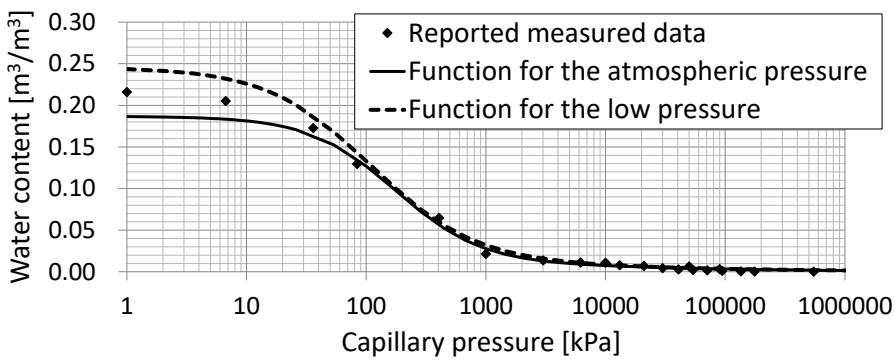

Figure 4. Adsorption isotherm for the atmospheric and extremely low air pressure.

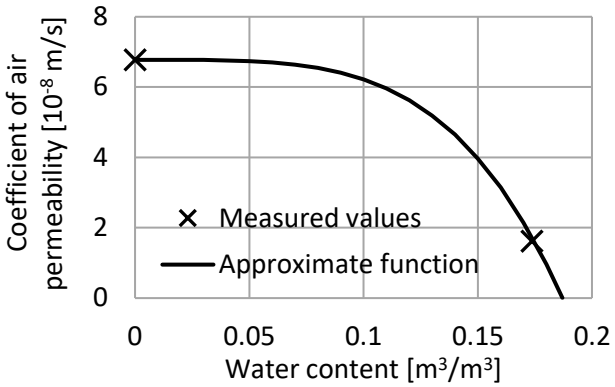

Figure 5. Air permeability used in the calculation.

3.2. Result and discussion

Figure 6 compares the calculated and measured water absorption rates, and figure 7 shows the calculated water content and air pressure in the material for calculation Case 3. The calculation results for Case 1 reasonably reproduced the results of the water uptake tests at atmospheric pressure, and the results for Case 2 show that the water diffusivity obtained from the water uptake tests at extremely low air pressure reproduces the water absorption rate. The comparison between the calculation results for Cases 2 and 3 demonstrates the significance of the effects of the air existing in the pores: the calculated rates of water absorption decreased, and the water content reached after the capillary absorption decreased for Case 3. The differences between the calculated results for Case 3 and the measured results at atmospheric pressure could be attributed to uncertainties in the material properties, especially for the low-pressure case.

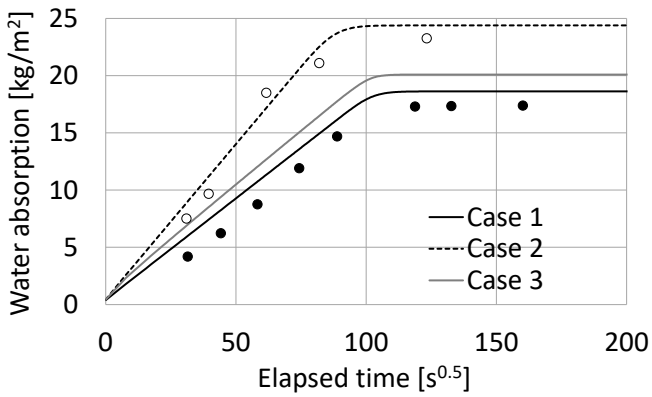

Figure 6. Comparison between the calculated (lines) and measured (markers) water absorption at the atmospheric and extremely low air pressure.

4. Conclusion

To understand the effects of air entrapment on water transfer in the high-water-saturation range near capillary saturation, we examined the water uptake at extremely low air pressure through both experiments and simulations. The experiments revealed that the low air pressure increased the water absorption rates of the brick and autoclaved aerated concrete specimens and the water content after capillary absorption, whereas the water uptake by the calcium silicate board specimens was not significantly affected. The differences among the materials can be attributed to differences in the extent of air compression in the pores, which depends on the pore structure of the material. Furthermore, the water transfer calculations using the water diffusion coefficient obtained from the water uptake test fairly reproduced the absorbed water mass at the negligibly low air pressure, and the simultaneous water and air transfer calculations based on Darcy's law and Boyle's law reproduced the water uptake tests at atmospheric pressure to some extent. The results helped us understand the characteristics of water transfer without the air entrapment effects and interaction between the air and liquid water in the pores.

In future research, the interaction between air and liquid water in porous building materials, as well as the material properties without air entrapment effects, will be further examined using more detailed experiments and simulations.

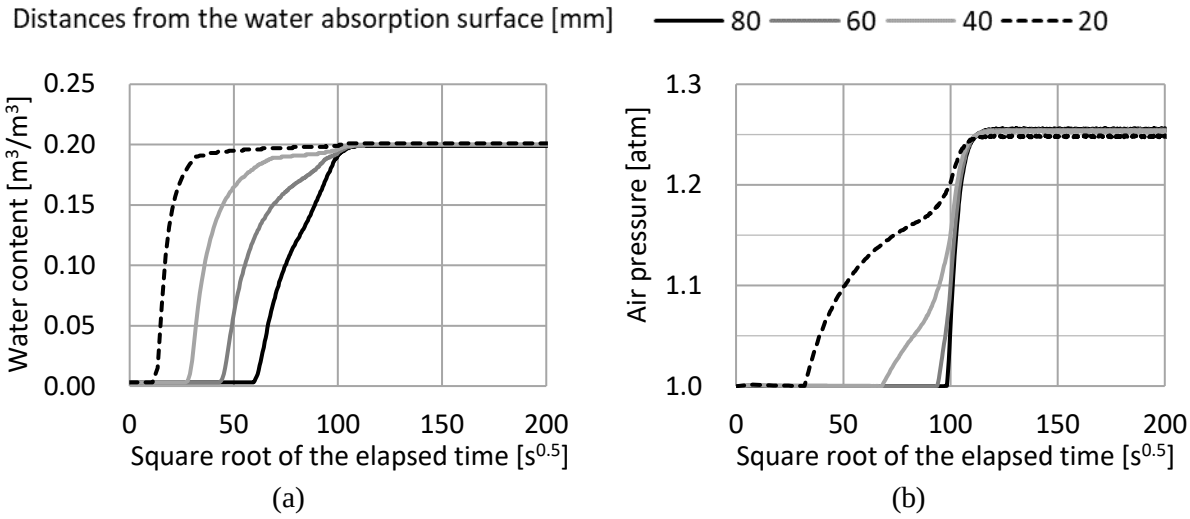

Figure 7. Calculated results of the (a) water content and (b) air pressure in the material.

Acknowledgments
This work was supported by JSPS KAKENHI Grant Numbers JP21K20462, JP23H01568, and JP23K13451.

References

[1] Fagerlund G 1977 *Mater. Struct.* **10** 217–30
[2] Janssen H, Vereecken E and Holúbek M 2015 *Energy Procedia* **78** 1490–94
[3] Vachaud G, Gaudet J P and Kuraz V 1974 *J. Hydrol.* **22** 89–108
[4] Descamps F 1997 *Continuum and discrete modelling of isothermal water and air flow in porous media* (Dissertation, Leuven: KU Leuven)
[5] Iba C and Hokoi S 2009 *J. ASTM Int.* **6** JAI102030
[6] Fukui K, Iba C, Hokoi S and Ogura D 2018 *Japan Archit. Rev.* **1** 538–47
[7] Fagerlund G 1994 *Predicting the service life of concrete exposed to frost action through a modelling of the water absorption process in the air-pore system (Report TVBM (Intern 7000-rapport); Vol. 7085)* (Lund: Division of Building Materials, LTH, Lund University)
[8] Evangelides C, Arampatzis G, Tsambali A-A, Tzanetaki E and Tzimopoulos C 2018 *Constr. Build. Mat.* **164** 830–36
[9] Kumaran M K 1996 *IEA Annex 24, Final Report, Vol. 3, Task 3: Material Properties* (Leuven: Laboratorium Bouwfysica, Department Burgerlijke Bouwkunde, KU Leuven)